Supplementary Information (SI)

Synergistic interfacial stabilization and kinetics acceleration in olivine cathodes enabled by rare-earth perovskite engineering

Xiangyue Chen,[‡a] Xinhui Li,[‡a] Wenji Yin,[b] Sijiang Hu,[b] Youwen Sun[c] and Tengfei Zhou*[a]*

X. Chen, X. Li, Prof. T. Zhou
a. Institutes of Physical Science and Information Technology, Anhui University, Hefei 230601, China
E-mail: tengfeiz@ahu.edu.cn

W Yin, Prof. S. Hu
b. Guangxi Key Laboratory of Low Carbon Energy Material, Guangxi Normal University, Guilin, 541004, China

Prof. Y. Sun
c. State Key Laboratory of Opto-Electronic Information Acquisition and Protection Technology, Anhui University, Hefei, China. E-mail: ywsun@ahu.edu.cn

Experimental Procedures：

Preparation of Pristine LMFP/C: $LiMn_{0.6}Fe_{0.4}PO_4/C$ was synthesized by a solvothermal process with stoichiometric precursors ($LiOH·H_2O$, $FeSO_4·7H_2O$, $MnSO_4·H_2O$, H_3PO_4 in a 3.0: 0.4: 0.6: 1.0 molar ratio) dissolved in an ethylene glycol/deionized water mixed solvent, with the addition of small amounts of L-ascorbic acid and CTAB. The precursor, obtained from a solvothermal reaction at 180 °C for 15 h, was coated with sucrose and then calcined at 700 °C for 5 h under an Ar/H_2 atmosphere to yield the final LMFP/C.

Fabrication of LSM Powders: $La_{0.8}Sr_{0.2}MnO_3$ was synthesized via a solution-based process using $La(NO_3)_3·6H_2O$, $Sr(NO_3)_2$, and $Mn(NO_3)_2·4H_2O$ as the starting materials. Stoichiometric amounts of the La, Sr, and Mn precursors were dissolved sequentially in deionized water, forming a light pink solution. A mixture of ethylene glycol and cetyltrimethylammonium bromide (CTAB) was then added under stirring, during which the solution color gradually turned brown. The resulting precipitate was collected by centrifugation, thoroughly washed with deionized water and ethanol, and dried. The obtained powder was then calcined under an Ar atmosphere for 5 hours at different temperatures (600, 650, 700, 800, and 900 °C) to yield the final LSM products.

Surface Coating: Disperse LSM with different mass fractions (0, 0.25, 1, 3, and 5 wt%) into LMFP/C in an anhydrous process, stir the mixture at room temperature until a paste is formed, then dry it in an oven. The resulting powder is sintered at 400 ℃ for 4 hours under an Ar/H_2 atmosphere to obtain samples co-coated with LSM and carbon, denoted as LMFP/C, LMFP/C-LSM0.25, LMFP/C-LSM1, LMFP/C-LSM3, LMFP/C-LSM5, respectively.

Material Characterization: The crystal structure of the material was characterized by X-ray diffraction (XRD) using a Cu Kα radiation source (λ = 1.5418 Å) with a scan rate of 2°/min over a 2θ range of 10° to 80°. The obtained data were analyzed using Jade 9.0 software. The morphology and microstructure of the samples were systematically investigated using field emission scanning electron microscopy (FESEM), transmission electron microscopy (TEM), and aberration-corrected transmission electron microscopy (AC-TEM). Elemental composition and distribution were characterized by energy-dispersive X-ray spectroscopy (EDS) mapping. The surface elemental

composition and chemical valence states of the materials were analyzed by X-ray photoelectron spectroscopy (XPS), with all XPS spectra calibrated for charge effects using the C 1s standard binding energy (284.8 eV). In addition, the L-edge absorption spectra of Fe and Mn were measured by synchrotron-based X-ray absorption spectroscopy (XAS) to analyze their local electronic structures and chemical valence states.

Electrochemical Measurements: The preparation of the positive electrode sheet was conducted as follows: the obtained positive electrode material served as the active material, Ketjen black as the conductive additive, and PVDF as the binder. They were mixed at a mass ratio of active material: conductive additive: binder = 8: 1: 1, with NMP added as the dispersant. After homogenization using a planetary mixer with defoaming function, the slurry was uniformly coated onto an aluminum foil current collector using a rod coating machine. The coated foil was then dried in a vacuum oven at 80 °C for 12 h. The dried electrode sheet was punched into disks with a diameter of 16 mm using a manual disc cutter, and disks with uniform coating thickness were selected as the positive electrode sheets, which were then weighed for battery assembly. The mass loading of the active material was controlled within 1.8-2.5 $mg \cdot cm^{-2}$. In an Ar-filled glovebox, CR2032 coin-type cells were assembled in the following order: positive electrode case, positive electrode sheet, electrolyte, separator, electrolyte, lithium sheet (negative electrode), spacer, spring, and negative electrode case. The separator used was Celgard 2325 (PP2325), the negative electrode was a metallic lithium sheet, and the electrolyte was 1 M $LiPF_6$ in DMC : EC : EMC = 1: 1: 1 by volume. Electrochemical tests were all conducted at room temperature (25 °C). Rate capability, long-term cycling, and galvanostatic charge–discharge tests were performed using a Neware battery testing system within a voltage range of 2.5-4.5 V. Cyclic voltammetry (CV) and electrochemical impedance spectroscopy (EIS) were conducted on a Donghua electrochemical workstation. CV tests were carried out in the voltage range of 2.5-4.5 V at scan rates of 0.1, 0.5, 1.0, 1.5, and 2.0 $mV \cdot s^{-1}$, respectively. EIS measurements were performed in a frequency range of 0.01-100,000 Hz with an amplitude of 5 mV.

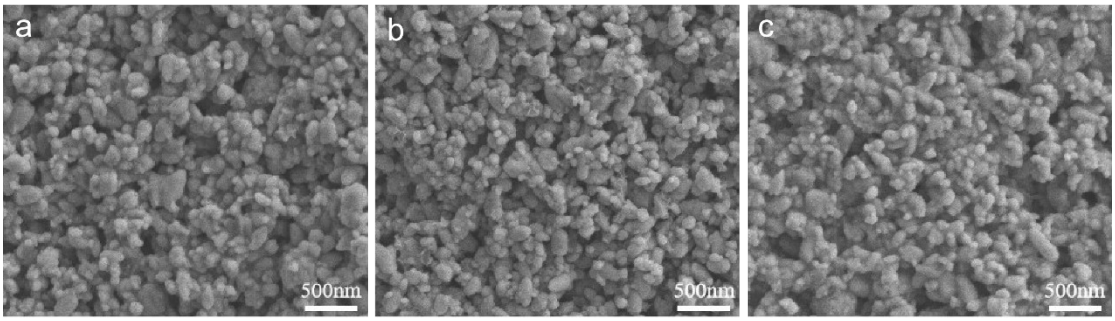

Figure S1. SEM images of (a) LMFP/C, (b) LMFP/C-LSM1, and (c) LMFP/C-LSM3.

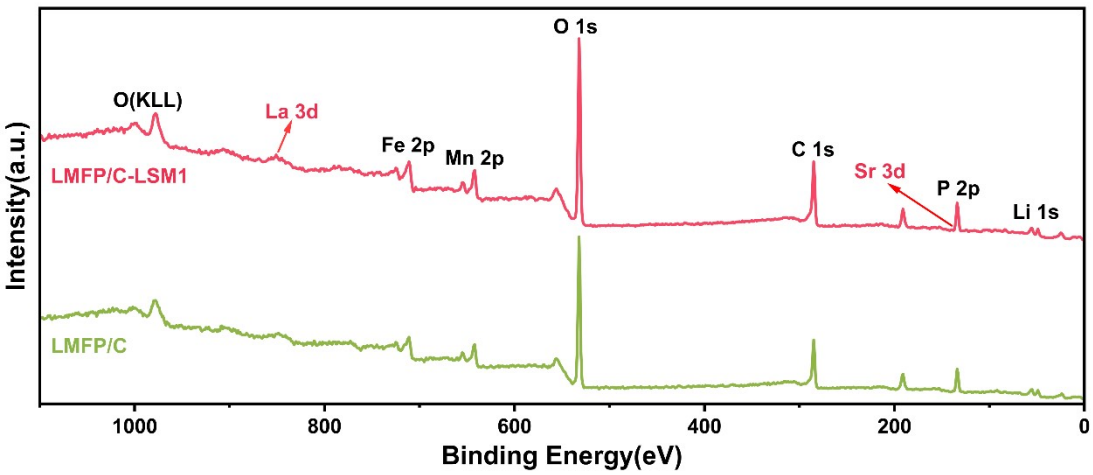

Figure S2. XPS full spectra of LMFP/C and LMFP/C-LSM1.

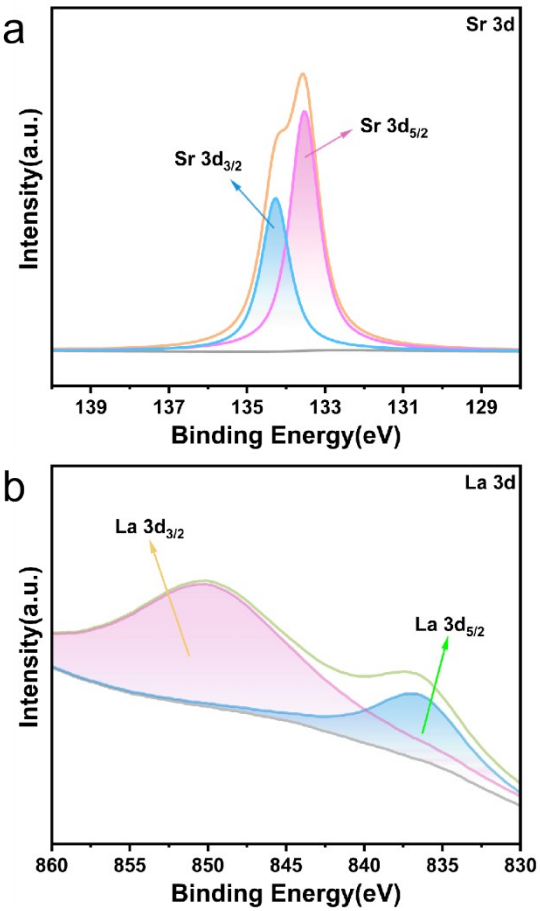

Figure S3. (a) Sr 3d XPS spectrum of LMFP/C-LSM1, (b) La 3d XPS spectrum of LMFP/C-LSM1.

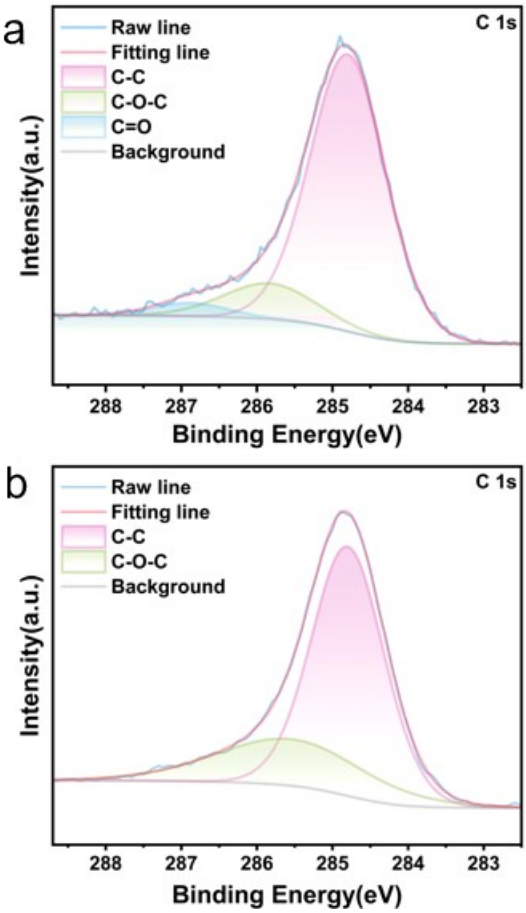

Figure S4. High-resolution XPS spectra of C 1s. (a) LMFP/C, (b) LMFP/C-LSM1.

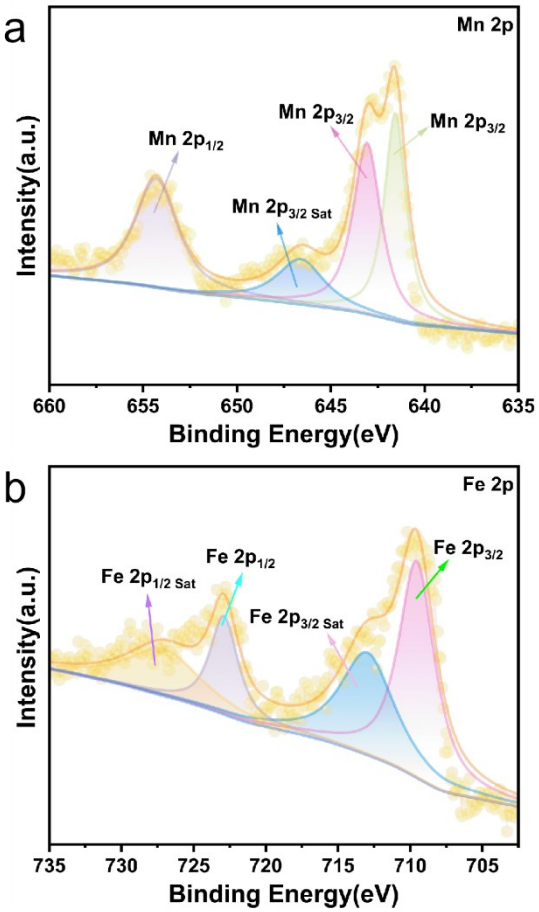

Figure S5. High-resolution XPS spectra of Fe 2p. (a) LMFP/C, (b) LMFP/C-LSM1.

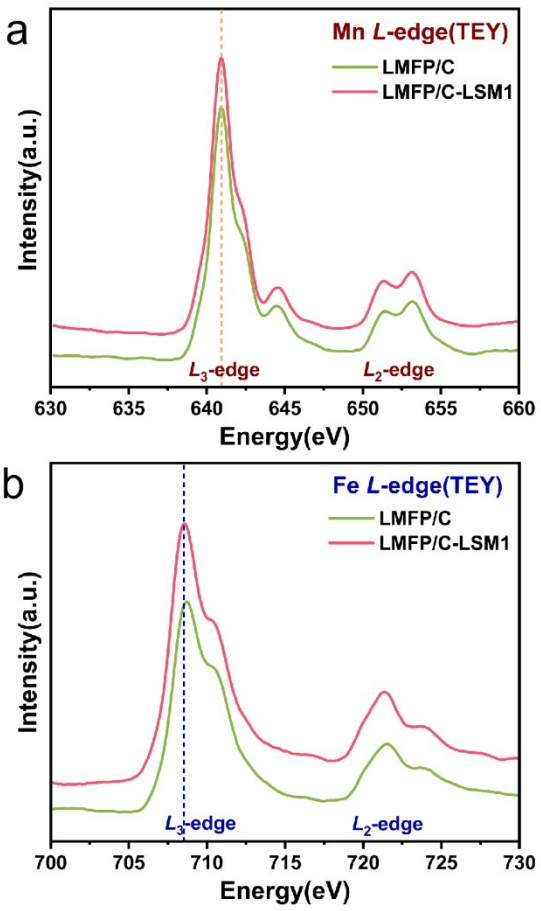

Figure S6. Comparison of synchrotron X-ray absorption spectra (XAS) acquired in total electron yield (TEY) mode for LMFP/C. (a) Mn L-edge, (b) Fe L-edge.

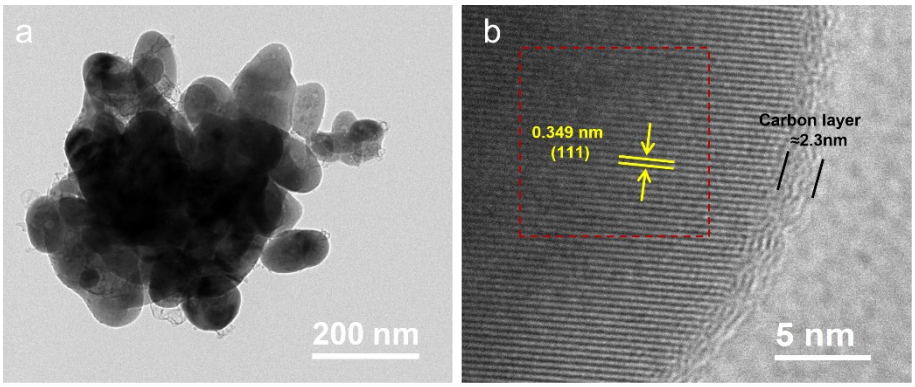

Figure S7. (a) TEM image and (b) HRTEM image of the LMFP/C sample.

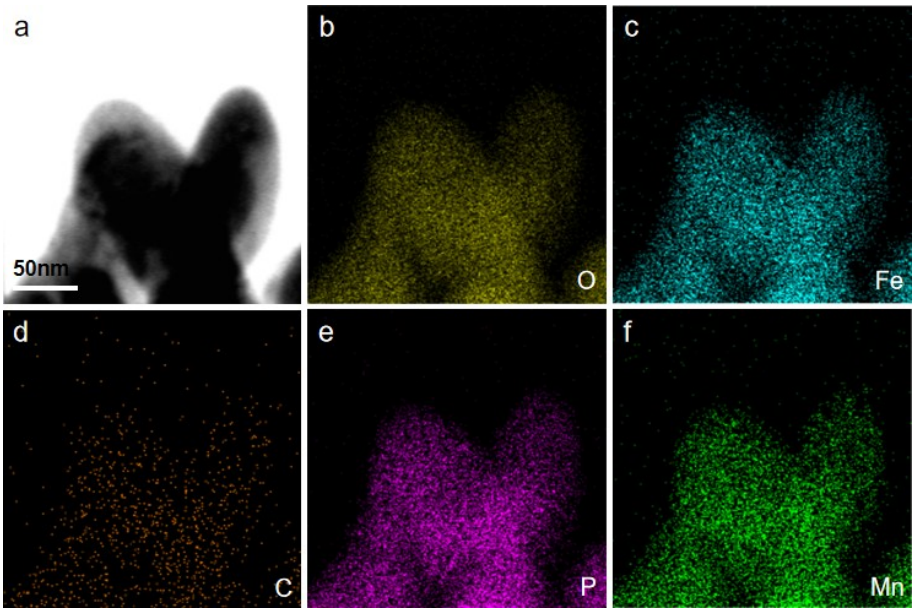

Figure S8. HRTEM image and EDS elemental mapping of LMFP/C: (a) HRTEM image, (b) O, (c) Fe, (d) C, (e) P, (f) Mn.

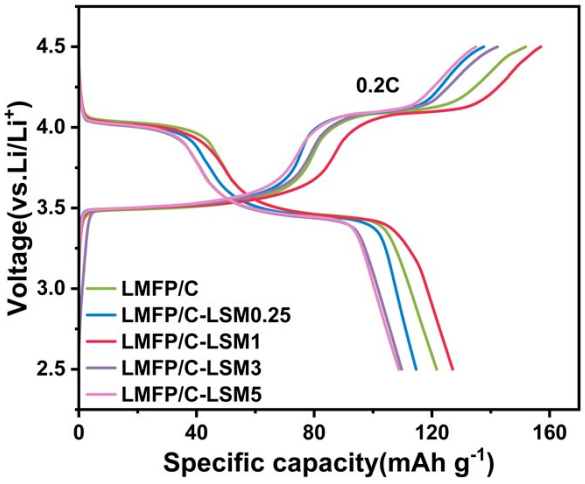

Figure S9. Initial charge/discharge curves of the LMFP/C-LSM composite at 0.2C.

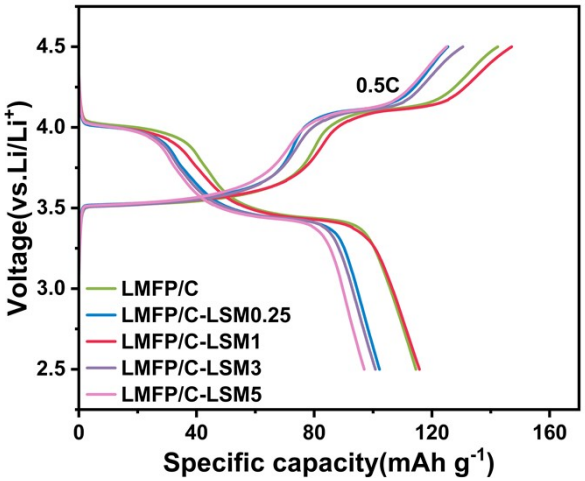

Figure S10. Initial charge/discharge curves of the LMFP/C-LSM composite at 0.5C.

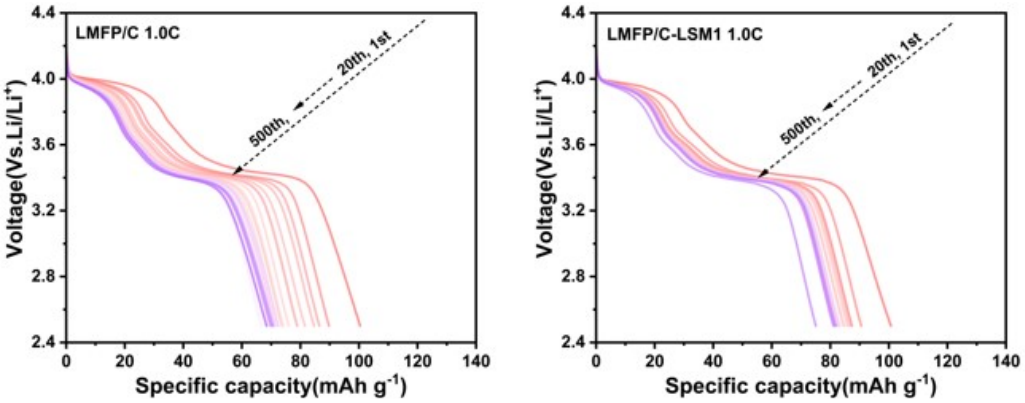

Figure S11. Voltage–discharge capacity profiles of LMFP/C and LMFP/C-LSM1 at 1.0C.

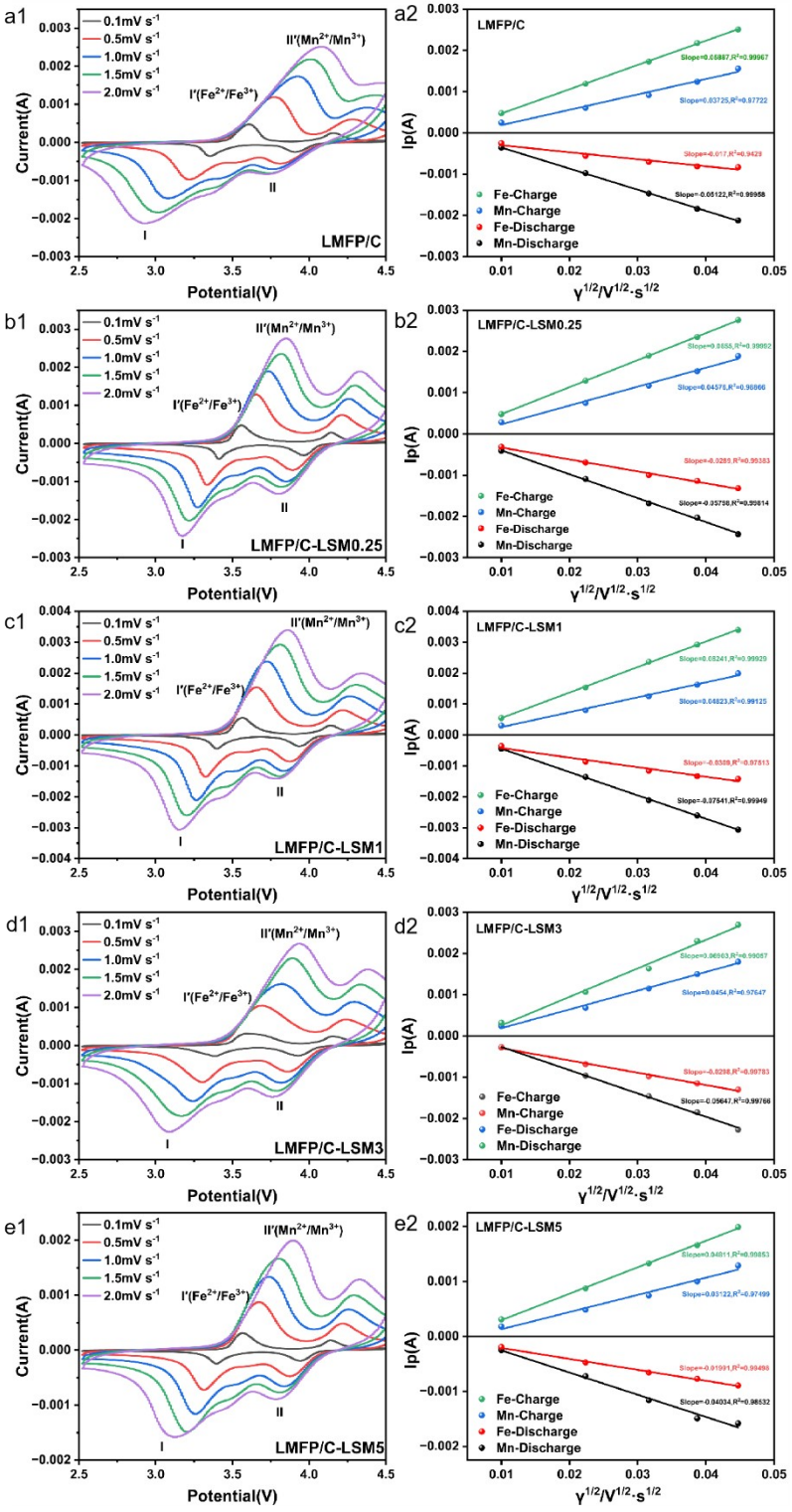

Figure S12. CV curve of 0.1-2.0 mV s^{-1} and linear relationship between positive/negative peak current and square root of scanning rate: (a1-a2) LMFP/C, (b1-b2) LMFP/C-LSM0.25, (c1-c2) LMFP/C-LSM1, (d1-d2) LMFP/C-LSM3, (e1-e2) LMFP/C-LSM5.

Table S1. The Li^+ diffusion coefficient derived from the Randles–Sevcik equation.

D_{Li} (cm^2/s)	Mn charge	Mn discharge	Fe charge	Fe discharge
LMFP/C	9.57×10^{-12}	2.39×10^{-11}	1.81×10^{-11}	1.99×10^{-12}
LMFP/C-LSM0.25	1.44×10^{-11}	2.96×10^{-11}	2.32×10^{-11}	5.76×10^{-12}
LMFP/C-LSM1	1.60×10^{-11}	4.68×10^{-11}	3.92×10^{-11}	6.58×10^{-12}
LMFP/C-LSM3	1.42×10^{-11}	3.29×10^{-11}	2.20×10^{-11}	6.13×10^{-12}
LMFP/C-LSM5	6.72×10^{-12}	1.60×10^{-11}	1.12×10^{-11}	2.73×10^{-12}

Table S2. Electrochemical performance comparison of LMFP-based cathodes between this work and previous reports.

Samples	Specific capacity	Cycling stability	Ref.
$LiMn_{0.8}Fe_{0.2}PO_4$/C	130.5mAh g^{-1} (0.1C)	95.5% (200 cycles, 0.5C)	[1]
LMFP/C	132mAh g^{-1} (1C)	95.12% (150 cycles, 1C)	[2]
LMFP/C	142mAh g^{-1} (1C)	67% (200 cycles, 5C)	[3]
C/LMFP@LLTO	131.3mAh g^{-1} (5C)	81% (100 cycles, 5C)	[4]
LMFP@Nb-Mg co-doped	129.5mAh g^{-1} (1C)	99% (300 cycles, 2C)	[5]
$LiMn_{0.6}Fe_{0.4}PO_4$/C	113.1mAh g^{-1}(0.5C), 60.0mAh g^{-1}(10C)	83.3% (1000 cycles, 10C)	[6]
$LiMn_{0.6}Fe_{0.4}PO_4$/GO	140.3mAh g^{-1} (0.05C), 116mAh g^{-1} (1C)	98% (21 cycles, 0.05C)	[7]
$LiMn_{0.8}Fe_{0.2}PO_4$/NMC	140mAh g^{-1} (0.2C)	95% (100 cycles, 1 C)	[8]
LFMP/RGO	148mAh g^{-1} (0.1C)	97% (100cycles, 0.1C)	[9]
$LiMn_{0.5}Fe_{0.5}PO_4$@LiAlO(5 wt%)@C	137.6mAh g^{-1} (0.05C), 113.2mAh g^{-1}(5C)	86.4% (100 cycles, 5C)	[10]
LMFP/C@MXene	139mAh g^{-1} (1C)	91.26% (600 cycles, 5C)	[11]
LMFP/C-LSM1	148.55mAh g^{-1} (0.1C)	79.1% (500 cycles, 2C)	This work

[1] Y. Wang, F. Yong, Z. Wang, M. Wang, Q. Peng, M. Zhao, Z. Chen, Q. Huang, S. Yang and F. Yu, *ACS Appl. Nano Mater.,* 2024, **7**, 4024–4034.

[2] H. Lei, K. Zhou, Y. Li, L. Yu, W. Chen and Y. Wu, *J. Power Sources*, 2025, **649**, 237476.

[3] M. Ratynski, M. Winkowska-Struzik, D. Buchberger, B. Hamankiewicz, M. Krajewski and A. Czerwinski, *ACS Appl. Energy Mater.* , 2025, **8**, 11053–11067.

[4] H. Chang, Y. Li, Z. Fang, J. Qu, Y. Zhu and T. Yi, *ACS Appl. Mater. Interfaces*, 2021, **13**, 33102–33111.

[5] P. Vanaphuti and A. Manthiram, *Small*, 2024, **20**, 2404878.

[6] J. Chen, N. Zhao, G. Li, T. Jia, D. Shi, Y. Zhao, X. Wang and F. Guo, *J. Solid State Electrochem.*, 2015, **19**, 1535-1540.

[7] C. Xu, L. Li, F. Qiu, C. An, Y. Xu, Y. Wang, Y. Wang, L. Jiao and H. Yuan, *J. Energy Chem.*, 2014, **23**, 397-402.

[8] X. Zhang, M. Hou, A.G. Tamirate, H. Zhu, C. Wang and Y. Xia, *J. Power Sources*, 2020, **448**, 227438.

[9] C. Rossou, K. Raju, H. Zheng and K. Ozoemena, *Curr. Appl Phys.*, 2017, **123**, 769.

[10] T. Yi, Y. Li, Z. Fang, P. Cui, S. Luo, Y. Xie. *J. Materiomics*, 2020, **6**, 33-44.

[11] G. Tian, S. Yan, R. Mao, Y. Cui, M. Tian, D. Yang, P. Cheng, J. Zhang, J. Xiang and N. Tang, *J. Energy Storage*, 2026, **162**, 121690.